Autonomous Source Discovery and Navigation in Complicated Environments

Yanina Landa[1], Haochong Shen[2], Ryo Takei[1], and Yen-Hsi R. Tsai[3]

Abstract— An autonomous robotic system (*observer*) is supposed to discover the location of a signal source, based on measurements from an onboard sensor, and place it under its line-of-sight in an efficient manner. The environment contains impenetrable obstacles that should be avoided along the robot's path. We present an adaptive algorithm for determining the measurement locations and, ultimately, the source location. Specifically, we implement the extension of the reciprocity-based source discovery algorithm [7], to noisy signal data. A Hamilton-Jacobi value function [34] controls the observer's motion, while taking the obstacles and the observer's heading and turning radius into account. An economical car-based platform [27] is used to validate our algorithm and demonstrate its efficiency.

I. INTRODUCTION

We consider an application that uses remote sensing and sensor deployment to discover a threat target. The target is a source that emits a remotely measurable signal (biochemical concentration, heat, sound, *etc.*). The goal is to design a robust algorithm that determines how the robot should navigate through the environment, and where along its path it should take measurements so that the objective of discovering a signal source and its surveillance can be achieved efficiently.

In this paper we present the experimental results based on the strategy discussed in [7]. We furthermore introduce the probability based imaging function to take into account the significant amount of noise in the measurements of the signal. As the result of our search strategy, a sequence of signal measurement locations is produced. To navigate the robot to the next observing position we propose a motion planner based Hamilton-Jacobi (HJ) equation [34].

The outline of the paper is as follows. In section II we present some of the existing techniques to solve the inverse problems in source discovery along with conventional algorithms for steering the autonomous vehicles in complicated environments. Then, in section III we describe the reciprocity-based source discovery algorithm, first introduced in [7], and its extension to noisy signal data. Section IV discusses the application of HJ formulation [34] to path planning. In section V we introduce the testbed and the robot-vehicle used for navigation as well as the phototransistor reflective object sensor used to measure the signal. Finally, in section VI we propose two algorithms for source discovery

and compare the results of their implementation on the testbed.

II. RELATED WORK

When omitting the navigation considerations, source discovery can be roughly classified as an inverse source problem. Ling *et al.* [28] explore a situation in which they recover the exact locations of multiple sources in a Poisson equation, given an initial guess for the locations and Dirichlet data collected on the boundary of the domain. For inverse problems related to the heat equation with sources see [2] and [3]. Other related topics can be found in [8], [18], [29], [10], and [1]. The research settings discussed in this paper differ greatly from many typical inverse problems which assume simple domains and dense arrays of sensors at fixed locations. Instead, we consider complicated domains with non-convex obstacles, noisy signal data, the possibility of placing the sensors freely in the domain, and the necessary coupling with some motion planning.

Dynamic source discovery using local sensing is considered in [30]. Here, a group of sensor-equipped agents move in a swarm and use collaborative sensing to efficiently search for and locate targets in some bounded simply connected domain.

When the obstacles are unknown, the environment needs to be mapped out as the robot moves, so that attempts to take measurements inside the obstacles are avoided and the robot's path does not intersect obstacles. The previous work of [20], [22], [21], and [23] on mapping the obstacles in unknown domains using visibility is convenient in this regard. In [7], the authors extend the domain mapping algorithms of [20] and [21] for point source discovery in this kind of setting using an approach based on reciprocity of the linear partial differential operators as well as the maximum principle for the associated elliptic problems. In this paper, we consider a simpler scenario when the obstacles are known. However, with the addition of the range sensor (to detect and map the obstacles), it would be possible to extend the algorithm to regions with unknown obstacles. Furthermore, multiple sources may be considered, provided that they are well separated. This is the subject of our forthcoming publication.

A significant component of our experiment is navigating a car-based autonomous robot to a prescribed location while avoiding the obstacles. The car's limited steering angle must be taken into consideration when designing the motion control. A comprehensive presentation of motion planning techniques can be found in the book by Latombe [24]. Motion planning is a fundamental problem in robotics. In

[1]Dept. of Mathematics, University of California Los Angeles, Los Angeles, CA 90095 {ylanda, rtakei}@math.ucla.edu
[2]Dept. of Electrical Engineering, University of California Los Angeles, Los Angeles, CA 90095 hshen@ee.ucla.edu
[3]Dept. of Mathematics, University of Texas at Austin, Austin, TX 78704 ytsai@math.utexas.edu

the most general form, motion planning consists of finding a robot's path from a start position to a goal position, while avoiding obstacles and satisfying some constraints [24]. In [14], [15], [9], and [26] the authors provide a broad review of problems specific to the research in robotics.

A book by Laumond [25] focuses on motion planning for cars in cluttered environments. Barraquand and Latombe [6] developed a Lagrangian framework for the bang-bang steering principle, which allows only six actions for the car: move all the way to the left, to the right, or straight ahead, and the same actions with reverse velocity. The found path is optimal for the user's cost function and step size. Each cost function would produce a single path connecting the start and the target positions.

A large class of optimal path planning problems can be formulated as problems involving HJ equations [5], [11] and solved efficiently [36], [33], and [35]. We implement a control based on HJ equation [34] that produces a value function corresponding to a given target location. The value function contains the time-cost of traveling from *any* point in the domain outside the obstacles and *any* orientation of the car toward the target along the optimal path. This is the key difference of the suggested HJ formulation from the Lagrangian approach [6].

III. SOURCE DISCOVERY

The reciprocity-based source discovery algorithm from [7] is described below. Consider a bounded domain $D \subset \mathbb{R}^2$, which contains impenetrable obstacles $\Omega \subsetneq D$. Denote the region available for navigation by $D_\Omega := D \setminus \Omega$. Assume the signal from the point source propagates according to the Dirichlet problem for the Poisson equation:

$$\begin{cases} -\Delta u(x) & = & c\delta(x - S), \text{ in } D_\Omega \\ u(x) & = & 0, \text{ on } \partial D_\Omega \end{cases}, \qquad (1)$$

where on the right-hand side there is the delta function centered at the (unknown) source location $S \in D_\Omega$, magnified by $c > 0$. We assume that the strength of the source c is known and omit it from now on. One can view this partial differential equation (PDE) as giving a description of the steady state of a diffusion problem. We have chosen Dirichlet boundary conditions in this example, but our methods can be adapted to other common boundary conditions, such as Neumann boundary conditions. The mathematical formulation of general inverse source problems of this type is discussed in [7].

A first, rather simple approach would be, starting at a point $z_0 \in D_\Omega$, use gradient ascent to determine a sequence of sample locations that would guide the observer toward the source at S.

$$\dot{x}(t) = \nabla u\left(x(t)\right), \text{ with } x(0) = z_0. \qquad (2)$$

However, there are several drawbacks to this method. First, it only works in cases where the Green's function has a specific structure, such as in the case of Laplace operator (1). The gradient-based approach will not work if we deal with slightly more general equations of the type: $\nabla \cdot (a(x)\nabla u) = f$, where $a(x)$, for example, is periodic. Second, even for the Laplace operator, one can come up with a pathological configuration for the obstacles where the gradient vanishes at points other then the source. Furthermore, such an approach is highly inefficient in terms of the number of signal measurements required to discover the source. We present the results of an experiment based on gradient ascent in section VI, as a comparison to our proposed algorithm.

We continue with the algorithm implemented in this paper. At an observing location $z_1 \in D_\Omega$, we can measure the signal intensity $I_1 = u(z_1)$. Then, we look at the solution to the adjoint problem with the delta function centered at the observing position z_1:

$$\begin{cases} -\Delta v_1(x) & = & \delta(x - z_1), \text{ in } D_\Omega \\ v_1 & = & 0, \text{ on } \partial D_\Omega \end{cases}. \qquad (3)$$

Now, for $y \neq z_1$, we have

$$\begin{array}{rcl} v_1(y) & = & \int_{D_\Omega} \delta(x - y)v_1 dx = \int_{D_\Omega} v_1 \Delta u dx, \\ u(z_1) & = & \int_{D_\Omega} \delta(x - z_1)u dx = \int_{D_\Omega} u \Delta v_1 dx, \end{array} \qquad (4)$$

and, by the Green's identity, $v_1(y) = u(z_1) = I_1$. Therefore, the source must lie on the I_1 level set of v_1:

$$y \in \{x \in D_\Omega : v_1(x) = I_1\}. \qquad (5)$$

The intuitive idea behind the choice of (3) is that the signal strength measured by the observer remains the same even if we interchange the position of the observer and the source. Such reciprocity is embedded in the integration-by-parts (4).

Assume at the next location $z_2 \in D_\Omega$, the observer takes another measurement of signal intensity $I_2 = u(z_2)$. The function v_2 can be computed and the set of possible source locations may be narrowed down to

$$y \in \{v_1 = I_1\} \cap \{v_2 = I_2\}. \qquad (6)$$

This procedure can be repeated until the source location is uniquely identified at the intersection of all corresponding level sets.

The proposed strategy can handle obstacles of a rather large class, including very complicated non-convex shapes as in Fig. 1. The only constraint comes from the size of the underlying mesh used to obtain the solution to PDE (3), since the grid has to resolve the features of the obstacles. The discretization of the domain results in a simple system of linear equations. We refer the reader to [13] and [32] for a discussion and efficient methods for solving PDEs.

In order to be practical in typical applications the algorithm needs to be robust to noise in the data. We propose the extension of the above approach to handle the noise in signal measurements. Experimental results in section VI illustrate the performance of our method on the data obtained with the sensor described in section V.

Define the probability based imaging function corresponding to an observing location z_k by

$$p_k(x) := \exp\left(-\frac{(v_k(x) - I_k)^2}{\sigma^2}\right), \qquad (7)$$

where v_k is the solution of (3) corresponding to z_k, $I_k :=$ $u(z_k)$ is the intensity of the signal at z_k, and σ^2 is the variance of the noise in the measurement. Thus, p_k attains its maximum of 1 inside the region of possible source locations $\{x \in D_\Omega : v_k(x) = I_k\}$ and has a Gaussian drop-off, correlated with the variance of the noise σ^2, away from this region.

The cumulative probability imaging function corresponding to a set of distinct observing locations $\{z_1, \ldots, z_M\}$ can be defined as

$$P_M(x) := \frac{1}{M} \sum_{k=1}^{M} p_k(x). \tag{8}$$

After suitable normalization, one can see that the probability of the point source locating at the maximum of this function increases with the number of observations. We say that the source has been discovered when the area of the region that possibly contains the source, $\int_{D_\Omega} \chi_{\{P_M(x) \geq \epsilon\}} dx$, is less then the desired tolerance A_ϵ. Here, χ is the characteristic function of a set, and $0 < \epsilon < 1$ is a threshold parameter, defining the region of possible source locations.

IV. THE HAMILTON-JACOBI MOTION CONTROL

We wish to model the problem of optimally steering the vehicle with a fixed turning radius $\rho > 0$ from a starting point $(x_s, y_s) \in D_\Omega$ with orientation $\theta_s \in [0, 2\pi)$ to a target $(x_t, y_t) \in D_\Omega$. In this section we derive a HJ equation to model the value function for this problem that can be solved efficiently using a finite differences discretization on a rectangular grid. For a more detailed description see [34].

A. Formal Derivation of the HJ Equation

We will assume that the vehicle travels at a constant speed 1. Let $\mathcal{A}_{\rho,(x_s,y_s),\theta_s}$ denote the set of admissible paths from (x_s, y_s, θ_s), that is, paths that obey the given conditions of vehicular motion. Mathematically, this is the set of parametrized paths $\gamma = (\gamma_1, \gamma_2) : [0, \infty) \to D_\Omega$ such that for all $t > 0$

$$
\begin{aligned}
|\dot{\gamma}(t)| &= 1, \text{ car speed is 1,} \\
|\dot{\theta}(t)| &\leq \rho^{-1}, \text{ maximum turning radius is } \rho, \\
\gamma(0) &= (x_s, y_s), \text{ initial position,} \\
\theta(0) &= \theta_s, \text{ initial direction of motion,}
\end{aligned}
$$

where $\theta(t) = \tan^{-1}(\dot{\gamma}_2(t)/\dot{\gamma}_1(t))$ is the vehicle's direction of motion. Equivalently,

$$\dot{\gamma}(t) = (\cos(\theta(t)), \sin(\theta(t))). \tag{9}$$

Define the value function $\varphi : D_\Omega \times [0, 2\pi) \to \mathbb{R}^+ \cup \{0\}$:

$$\varphi(x, y, \theta) = \inf\{t : \gamma \in \mathcal{A}_{\rho,(x,y),\theta}, \gamma(t) = (x_s, y_s)\}. \tag{10}$$

Note that $\varphi(x_t, y_t, \theta) = 0$ for all $\theta \in [0, 2\pi)$.

From the value function, we can derive a corresponding dynamic programming principle [4]:

$$\varphi(x, y, \theta) = \inf_{\gamma \in \mathcal{A}_{\rho,(x,y),\theta}} \{\varphi(\gamma(t + \Delta t), \theta(t + \Delta t)) + \Delta t\}. \tag{11}$$

Rearranging the terms, dividing by Δt, and taking the limit $\Delta t \to 0$, we have,

$$-1 = \inf\{(\varphi_x, \varphi_y, \varphi_\theta) \cdot (\dot{\gamma}_1, \dot{\gamma}_2, \dot{\theta}) : |\dot{\gamma}| = 1, |\dot{\theta}| \leq \rho^{-1}\}, \tag{12}$$

where variable subscripts denote partial derivatives. Using (9) and the bang-bang principle $\dot{\theta} = \pm\rho^{-1}$, we arrive at the HJ equation

$$-1 = \cos(\theta)\varphi_x + \sin(\theta)\varphi_y - \rho^{-1}|\varphi_\theta|, \tag{13}$$

with the boundary condition

$$\varphi(x_t, y_t, \theta) = 0, \text{ for all } \theta \in [0, 2\pi). \tag{14}$$

To solve the above boundary value problem, we propose an upwind, monotone finite differences scheme on a three-dimensional uniform Cartesian grid. We refer the reader to [34], [31], [12], and [35] for more details on the chosen discretization of HJ equations.

B. Optimal Paths

The optimal paths coincide with the characteristic equations of (13). Thus, an optimal path satisfies the system of ordinary differential equations consisting of (9) and

$$\dot{\theta}(s) = \rho^{-1}\text{sign}\{\varphi_\theta\}. \tag{15}$$

To extract the unique path that passes through the starting point (x_s, y_s, θ_s) we solve:

$$
\begin{cases}
\dot{\gamma}(s) &= -(\cos(\theta(s)), \sin(\theta(s))), \\
\dot{\theta}(s) &= -\rho^{-1}\text{sign}\{\varphi_\theta\},
\end{cases} \tag{16}
$$

with initial condition

$$(\gamma(0), \theta(0)) = ((x_s, y_s), \theta_s). \tag{17}$$

Note that the value function contains the information to compute optimal paths from any orientation and any point in D_Ω to the target (x_t, y_t). This is a key difference of the HJ formulation from the Lagrangian approach in [9].

Numerically, the optimal paths can be computed by discretizing the initial value problem (16)-(17). We construct the path using a forward Euler discretization with a suitable chosen arc-length step until the path reaches (x_t, y_t) within some given tolerance. The values of φ and θ away from grid nodes are approximated by cubic interpolation of the nearby grid node values.

V. TESTBED AND SENSOR

The results in this paper were obtained using the second generation [27] of an economical micro-car testbed developed in [17]. The purpose of the testbed is to design a cost effective platform to study cooperative control and path planning strategies. The system includes a centralized data processing computer, an arena with the terrain and signal information, a micro-vehicle, and an overhead camera to track the vehicle on the floor.

The dimensions of the testbed floor are 140×140 cm. To represent the intensity of the signal at various locations, the floor is colored with the scales of gray according to the

solution of (1), with the lightest scale corresponding to the strongest signal as in Fig. 1. The obstacles are represented by the light gray contours.
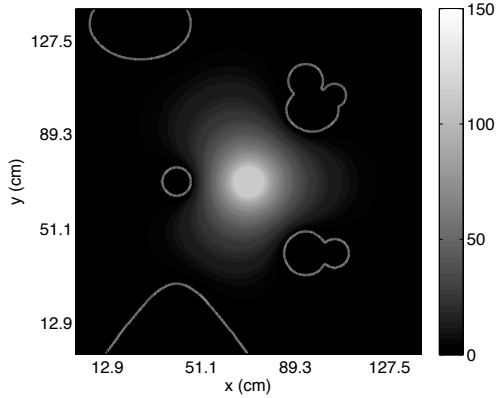

Fig. 1. Test arena with obstacles. Gray scale intensity corresponds to signal strength u, the solution of (1).

The micro-vehicle is composed of a car chassis, three layers of circuit boards, and an identification tag, encoding the vehicle's position and heading, on the top. The car is depicted in Fig. 2. It has dimensions $7 \times 3.8 \times 4.6$ cm and weighs 65 g with batteries. Equipped with a micro-processor, a wireless transceiver, and a phototransistor reflective object sensor, the vehicle is able to make simple motion decisions, broadcast information, and detect and measure the light reflectivity on the floor beneath it, which is then translated into signal intensity through calibration.
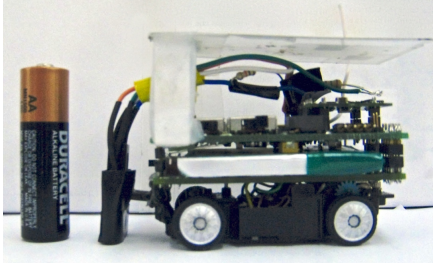

Fig. 2. Micro-vehicle equipped with a phototransistor reflective object sensor, pointing down.

We work with the sensor manufactured by Fairchild, model QRB1134. The sensor is mounted facing down, so that very little light comes between the sensor and the ground. This way we can insure the measurement of true light reflectivity of the gray scales beneath it. Here we describe the process of sensor data calibration. The sensor outputs the readings through the wireless radio transceiver at a rate 30 Hz. Sensor readings are produced by *Analog Digital Converter* (ADC), which outputs values proportional to voltage output ($V \times 204.8$). Fig. 3 represents sensor ADC output corresponding to gray scales ranging from 0 to 255. One can see that the curve flattens out after the gray scale reaches 185, that is, the sensor does not differentiate between gray scales brighter than 185. The estimated standard deviation of the noise is $\sigma = 12$, with the corresponding variance of σ^2.
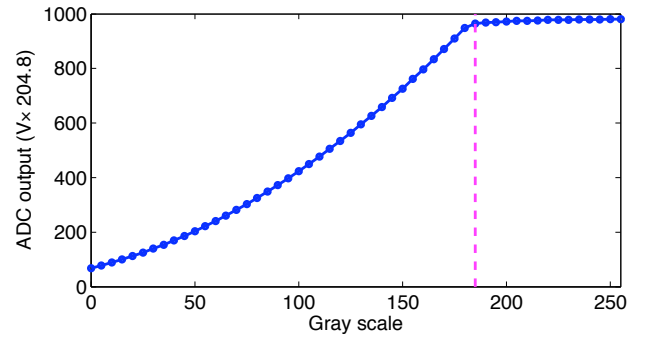

Fig. 3. Sensor ADC output corresponding to gray scales ranging from 0 (black) to 255 (white). The vertical line marks the working sensor range at the gray scale of 185.

VI. Algorithms, Experimental Results, and Discussion

In this section we are going to describe and compare the two algorithms for source detection: the reciprocity-based detection algorithm for Poisson equation (1) and the modified gradient-based algorithm. The outcomes of the experiments are discussed below.

A. Reciprocity-based Algorithm

We begin by introducing Algorithm 1 for detecting the source in Poisson equation (1). The results of the experiment are depicted in Fig. 4.

Algorithm 1 Reciprocity-based source discovery

1: $I := u(z)$: solution of (1) can be measured at any z.
2: set ϵ: threshold parameter.
3: set A_ϵ: desired tolerance.
4: set d: minimal separation between the observing locations in terms of Euclidean distance.
5: $k = 1$: number of observations.
6: $A = 0$: area of the region containing the source.
7: choose $z_1 \in D_\Omega$: first observation point.
8: **while** $0 \leq A < A_\epsilon$ **do**
9:      measure signal intensity $I_k := u(z_k)$.
10:     solve (3) for $v_k(x)$.
11:     compute $P_k(x)$ using (7) and (8).
12:     compute $A = \int_{D_\Omega} \chi_{\{P_M(x) \geq \epsilon\}} dx$.
13:     choose $z_{k+1} \in \{x \in D_\Omega : v_k(x) > u(z_k)\}$, which is the nearest to z_k, while dist $(z_{k+1}, \{z_1, \ldots, z_k\}) \geq d$.
14:     $k = k + 1$.
15: **end while**

The key idea behind the Algorithm 1, as described in section III, is to consider a sequence of solutions to adjoint problems (3) corresponding to different signal sampling locations. While the source has not been discovered, we measure the intensity of the signal I_k at an observing location z_k. Then, the adjoint problem (3) is solved and the probability imaging function (7) is constructed around $\{x \in D_\Omega : v_k(x) = I_k\}$, the level set of the solution v_k, marked by the black contours in Figs. 4. The colors ranging

from blue to red on the background of Figs. 4 correspond to values of the cumulative probability based imaging function defined in (8).

The region of possible source locations, bounded by the white curves in Figs. 4, is a neighborhood around the maximum of the cumulative probability imaging function (8). The size of the neighborhood depends on the variance σ^2 of the noise in the signal data. As the number of the observations increases, the area of the region of possible source locations shrinks down to a point, as can be seen from steps 6 and 7 of Fig. 4. The algorithm terminates when the area of the region containing the source is less then the desired tolerance. The magenta diamond in steps 6 and 7 marks the maximum of the cumulative probability imaging function (8), which is the estimated location of the source at (74.4580, 69.2660). The true coordinates of the source are (70.2100, 70.2100). Note, that the observer does not need to arrive to the source to determine its location.

In step 13 of Algorithm 1, the next observing location is selected. We choose z_{k+1} outside the level set $\{x \in D_\Omega : v_k(x) = I_k\}$. Heuristically, such a choice would result in a well-resolved intersection of the level sets at the source. Note that in steps 1 and 2 depicted in Fig. 4 the level sets $\{x \in D_\Omega : v_k(x) = I_k\}$ (depicted by black curves) do not pass through the source, which is located in the middle of the region. This occurs due to noise in the data, as the signal is sampled far from the source. However, as the observer proceeds, the level sets approach the true source location and, finally, in steps 6 and 7 they pass through the source. The probability imaging function allows us to consider wide regions instead of intersections of the level sets, adding robustness to our approach. The second condition in step 13 prevents the observer from returning to any of the previously visited cites.

To navigate the car to the next observing position, we choose the HJ motion control described in section IV. For each desired target location we calculate a three-dimensional value function (13)-(14). Since the map of the environment is known *a priori*, we chose to pre-compute the value functions at approximately 100 locations on the grid, approximately 12.7 cm apart (see Fig. 4), excluding the grid nodes inside the obstacles. This way, the value function for any target location generated by the algorithm could be approximated using the pre-computed values, saving computational time during the experiment. The nearest neighbor approximation turns out to be sufficient for our purposes, although more elaborate interpolation techniques, *e.g.* [16], could be implemented instead.

The value function allows us to efficiently compute optimal paths from any point in the domain to the target point via (16) and (17). Thus, the vehicle's steering direction can be quickly updated to correct the vehicle each time it slides away from its originally optimal path. The red circles in Figs. 4 mark the target observing locations where the signal is measured. The intermediate blue circles mark the positions where the optimal path was recomputed to adjust to the car's deviation from its original route. The distance between the blue circles is a fixed parameter obtained experimentally.

B. Gradient-ascent-based Algorithm

Below we describe Algorithm 2 based on the solution of (2). The key idea behind the algorithm is to navigate the car in the direction of the increasing gradient of the signal u (1), which is sampled along the path. The signal intensity u, is the same as in the previous experiment. A sample path leading to source discovery is depicted in Fig. 5.

Algorithm 2 Gradient-based source discovery

1: $I := u(z)$: solution of (1) can be measured at any z.
2: set $I_{\max}$: strongest signal value at the source.
3: set $I_{\min}$: threshold for weakest allowed signal.
4: set d: minimal separation between the observing locations with weak signal, in terms of Euclidean distance.
5: $k = 1$: number of observations.
6: choose $z_{1,1} \in D_\Omega$: first observation point.
7: measure $I_1 := u(z_{1,1})$.f
8: **while** $I_{k,1} < I_{\max}$ **do**
9:     **while** $I_{k,1} < I_{\min}$ **do**
10:         choose $z_{k+1,1} \in D_\Omega$, which is the nearest to z_k, while dist $(z_{k+1}, \{z_1, \ldots, z_k\}) \geq d$.
11:         $k = k + 1$.
12:     **end while**
13:     choose $z_{k,2}$ and $z_{k,3}$ in a small neighborhood of $z_{k,1}$.
14:     compute a linear approximation of $\nabla \tilde{u}(z_{k,1})$.
15:     $k = k + 1$.
16:     set $z_{k,1}$ along the direction of increasing $\nabla \tilde{u}(z_{k-1,1})$ using the bang-bang steering principle.
17:     measure signal strength $I_{k,1} := u(z_{k,1})$.
18: **end while**

We choose to measure the gradient of the signal only when the intensity of the signal is significantly greater than the standard deviation of the noise. Based on the data in Fig. 3, we set the minimal allowed signal $I_{\min} = 18$. While the measured signal is less than $I_{\min}$, we select the next observing location a distance $d > 0$ away from all the previous samples. Since the environment is bounded, the observer would end up in the region with a strong enough signal in finitely many steps. The HJ motion control from section IV is used to steer the vehicle. In Fig. 5, the path of the observer is depicted by the green curve connecting the steps generated by the HJ-based motion planner. The signal is sampled at the points marked by magenta circles.

Once the measured signal is sufficiently strong, the gradient can be used to steer the observer towards the source. We compute a linear approximation $\nabla \tilde{u}(z_{k,1})$ of the gradient, based on three measurements of the signal u in a small neighborhood of the observation point $z_{k,1}$. To accomplish this, the car steers a little in reverse to sample the signal at $z_{k,2}$ and then a little forward and to the side, to take the third sample at $z_{k,3}$. Fig. 5 depicts the estimated gradient directions with red arrows. We omit the corresponding sampling locations $z_{k,2}$ and $z_{k,3}$ for clarity.
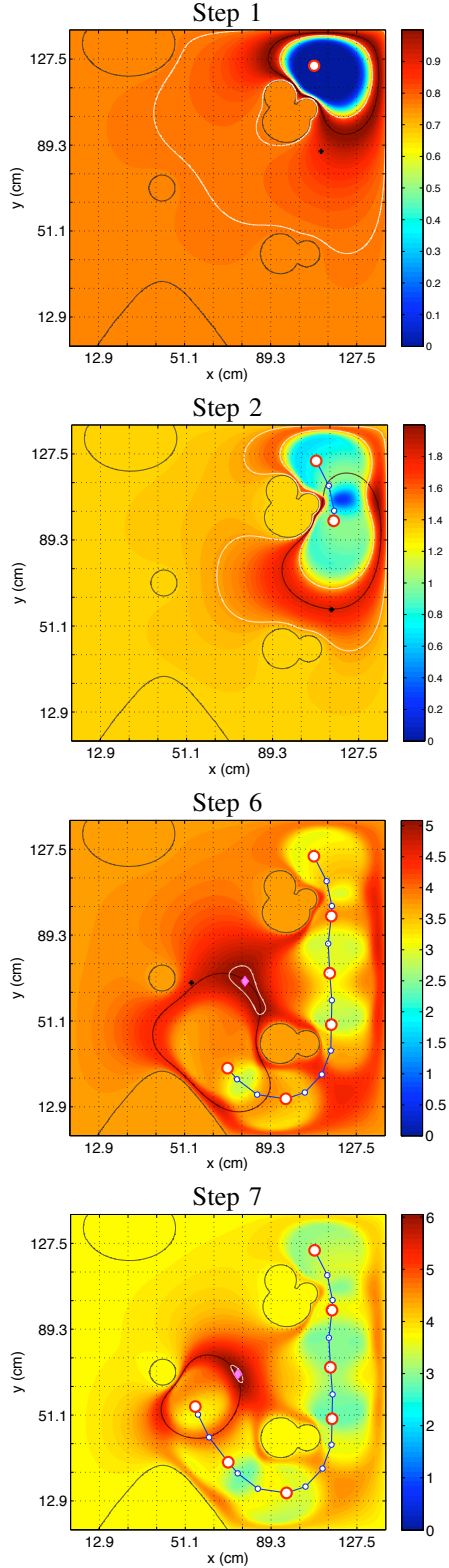
Fig. 4. Steps 1, 2, 6, and 7 of the source detection experiment based on Algorithm 1. The colored background illustrates cumulative probability imaging function (8). The path of the vehicle is marked with blue line segments connecting the steps generated by HJ controls (13) and (14). The signal is measured at red circles. The black cross marks the next measurement location (except for the last step). The black contour marks the level set $\{v_k(x) = u(z_k)\}$. The white contour bounds the region of possible source locations. The magenta diamond in steps 6 and 7 marks the maximum of the cumulative probability imaging function and corresponds to source position.
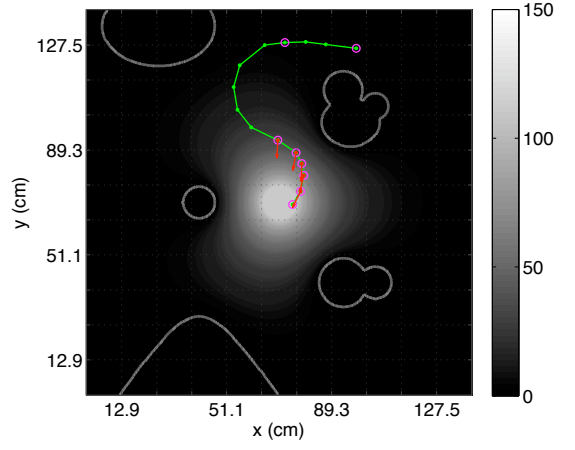

Fig. 5. Source detection based in Algorithm 2. The path of the observer is marked by green segments connecting the steps generated by HJ motion control. The signal is measured at magenta circles. The gradient is measured at red circles. The red arrows point in the direction of increasing gradient. The gray scale image on the background illustrates propagation of the signal in the environment.

From now on, the car navigates according to the gradient direction, using the bang-bang steering principle described in section II. That is, from the six possible directions, the observer chooses the one nearest to the direction of increasing gradient. The step size is chosen small enough as to not overshoot the source. Note that in Fig. 5 the trajectory of the car (green) initially does not coincide with the direction of the gradients (red arrows). This is due to the fact that the vehicle's orientation does not coincide with the gradient direction. Both directions become aligned as the car steers closer toward the source. The car stops once it reaches the source, that is, when the signal is stronger than a desired tolerance $I_{\max}$. The estimated source location in Fig. 5 is (75.1660, 69.5000).

C. Discussion

Note, the observer must travel to the source in order to discover its location using Algorithm 2, whereas this is not at all necessary when using Algorithm 1. Also, observe that eight measurements of the signal and five measurements of the gradient (which is a total of eighteen samplings of the signal) are required to discover the source with Algorithm 2. In contrast, only seven measurements are sufficient with Algorithm 1. The same starting position of the observer is used in both experiments.

Let us further remark that Algorithm 1 may be modified to include the gradient information of the signal, see [7] for details. While in this paper we assume the maximum strength of the signal is known, it is possible to recover the strength of the signal using the approach described in [7]. The case of multiple signals of varying strengths will be considered in the forthcoming publication.

The addition of the range sensor would make it possible to consider an experiment of discovering a point source in an unknown domain with obstacles [7]. The range sensor would be used to collect point clouds from the surfaces

of solid obstacles in the environment, as was done in [21]. The visibility algorithm from [20] and [22] would then be combined with the source detection algorithm to explore the environment while looking for the source. Collaboration of multiple observers could also be implemented for faster and more efficient source discovery and tracking. Once the signal is discovered, a boundary tracking method, *e.g.*, [19] could be implemented for further tracking and surveillance of the contaminated region.

VII. Acknowledgements

References

[1] V. Akcelik, G. Biros, O. Ghattas, K. R. Long, and B. Waanders. A variational finite element method for source inversion for convective-diffusive transport. *Finite Elem. Anal. Des.*, 39(8):683–705, 2003.

[2] A. El Badia and T. Ha-Duonh. On an inverse problem for the heat equation. application to a pollution detection problem. *J. Inverse Ill-Posed Probl.*, 10(6):585–599, 2002.

[3] A. El Badia, T. Ha-Duonh, and A. Hamdi. Identification of point source in a linear advection-dispersion-reaction equation: application to a pollution source problem. *Inverse Problems*, 21(3):1121–1136, 2005.

[4] M. Bardi. *Some applications of viscosity solutions to optimal control and differential games*, volume 1660/1997 of *Lecture Notes in Mathematics*, pages 44–97. Springer Berlin / Heidelberg, 1997.

[5] M. Bardi and I. Capuzzo-Dolcetta. *Optimal Control and Viscosity Solutions of Hamilton-Jacobi-Bellman Equations*. Birkhauser Boston Inc., Boston, MA, 1997.

[6] J. Barraquand and J. C. Latombe. Nonholonomic multibody mobile robots: Controllability and motion planning in presence of obstacles. *Algorithmica*, 10:121–155, 1993.

[7] M. Burger, Y. Landa, N. Tanushev, and R. Tsai. Discovering point sources in unknown environments. In *WAFR'08: The 8th International Workshop on the Algorithmic Foundations of Robotics*, December 2008.

[8] Y. Cheng and T. Singh. Source term estimation using convex optimization. In *2008 11th International Conference on Information Fusion*, pages 1–8, 2008.

[9] H. Choset, K. M. Lynch, S. Hutchinson, G. Kantor, W. Burgard, L. E. Kavraki, and S. Thurn. *Principles of Robot Motion*. MIT Press, 2005.

[10] M. Choulli and M. Yamamoto. Some stability estimates in determining sources and coefficients. *J. Inverse Ill-Posed Probl.*, 14(4):355–373, 2006.

[11] L. C. Evans. *Partial Differential Equations*. Amer. Math. Soc., 1998.

[12] M. Falcone and R. Ferrretti. Semi-Lagrangian schemes for Hamilton-Jacobi equations, discrete representation formulae and Godunov methods. *J. Comput. Phys.*, 175(2):559–575, 2002.

[13] F. Gibou, R. P. Fedkiw, L.-T. Cheng, and M. Kang. A second-order-accurate symmetric discretization of the Poisson equation on irregular domains. *J. Comput. Phys.*, 176(1):205–227, 2002.

[14] D. Halperin, L. E. Kavraki, and J. C. Latombe. Robot algorithms. In *Handbook of Algorithms and Theory of Computation*. CRC Press, Boca Raton, FL, 1999.

[15] D. Halperin, L. E. Kavraki, and J. C. Latombe. Robotics. In J. E. Goodman and J. O'Rourke, editors, *Handbook of Discrete and Computational Geometry*. CRC Press, Boca Raton, FL, 2004.

[16] A. Harten, B. Engquist, S. Osher, and S. R. Chakravarthy. Uniformly high order accurate essentially non-oscillatory schemes, III. *J. Comput. Phys.*, 71:231–303, 1987.

[17] C. H. Hsieh, Y.-L. Chuang anf Y. Huang, K. K. Leung, A. L. Bertozzi, and E. Frazzoli. An economical micro-car testbed for validation of cooperative control strategies. In *Proc. of the 2006 American Control Conference, ACC'06*, pages 1446–1451, 2006.

[18] V. Isakov. Inverse parabolic problems with the final overdetermination. *Comm. Pure Appl. Math.*, 44(2):185–209, 1991.

[19] Z. Jin and A. L. Bertozzi. Environmental boundary tracking and estimation using multiple autonomous vehicles. In *IEEE Conference on Decision and Control*, pages 4918–4923, 2007.

[20] Y. Landa. *Visibility of point clouds and exploratory path planning in unknown environments*. PhD thesis, UCLA, 2008.

[21] Y. Landa, D. Galkowski, Y. R. Huang, A. Joshi, C. Lee, K. K. Leung, G. Malla, J. Treanor, V. Voroninski, A. L. Bertozzi, and R. Tsai. Robotic path planning and visibility with limited sensor data. In *Proceedings of the 2007 American Control Conference, ACC'07*, 2007.

[22] Y. Landa and R. Tsai. Visibility of point clouds and exploratory path planning in unknown environments. *Comm. Math. Sci.*, 6(4):881–913, 2008.

[23] Y. Landa, R. Tsai, and L.-T. Cheng. Visibility of point clouds and mapping of unknown environments. In *Advanced Concepts for Intelligent Vision Systems, 2006. ACIVS'06*, pages 1014–1025, 2006.

[24] J.-C. Latombe. *Robot motion planning*. Kluwer Academic Publishers, 1991.

[25] J.-P. Laumond. *Robot motion planning and control*. Springer, 1998.

[26] S. M. LaValle. *Planning Algorithms*. Cambridge University Press, 2006.

[27] K. K. Leung, C. H. Hsieh, Y. R. Huang, A. Joshi, V. Voroninski, and A. L. Bertozzi. A second generation micro-vehicle testbed for cooperative control and sensing strategies. In *American Control Conference, 2007. ACC'07*, pages 1900–1907, 2007.

[28] L. Ling, Y. C. Hon, and M. Yamamoto. Inverse source indentification for Poisson equation. *Inverse Problems in Science and Engineering*, 13(4):433–447, 2005.

[29] L. Ling, M. Yamamoto, Y. C. Hon, and T. Takeuchi. Identification of source locations in two dimensional heat equations. *Inverse Problems*, 22:1289–1305, 2006.

[30] W. Liu, M. B. Short, and A. L. Bertozzi. Collaborative searching through swarming. Preprint, 2009.

[31] A. Oberman. Convergent difference schemes for nonlinear elliptic and parabolic equations: Hamilton-Jacobi equations and free boundary problem. *SIAM J. Numerical Analysis*, 44(2):879–895, 2006.

[32] S. Osher and R. P. Fedkiw. Level set methods: an overview and some recent results. *J. Comput. Phys.*, 169(2):463–502, 2001.

[33] J. A. Sethian. Evolving interfaces in computational geometry, fluid mechanics, computer vision, and materials science. In *Level Set Methods and Fast Marching Methods*. Cambridge University Press, second edition, 1999.

[34] R. Takei, Y.-H. R. Tsai, H. Shen, and Y. Landa. A practical path-planning algorithm for a simple car: a Hamilton-Jacobi approach. Preprint, September 2009.

[35] Y.-H. R. Tsai, L. T. Cheng, S. Osher, and H. K. Zhao. Fast sweeping algorithms for a class of Hamilton-Jacobi equations. *SIAM J. Numerical Analysis*, 41(2):673–694, 2003.

[36] J. Tsitsiklis. Efficient algorithms for globally optimal trajectories. *IEEE Trans. on Auto. Control*, 40(9):1528–1538, 1995.